Ionization and Dissociation Processes of Pyrrolidine in Intense Femtosecond Laser Field†

Qiaoqiao Wang, Di Wu, Dongdong Zhang, Mingxing Jin, Fuchun Liu, Hang Liu, Zhan Hu, and Dajun Ding*

Institute of Atomic and Molecular Physics, Jilin University, Changchun 130012, P. R. China

Hirobumi Mineo,‡ Yuri A. Dyakov,§ Yoshiaki Teranishi,|| Sheng Der Chao,‡ A. M. Mebel,⊥ and Sheng Hsien Lin§,||

Institute of Applied Mechanics, National Taiwan University, Taipei 106, Taiwan, Institute of Atomic and Molecular Sciences, Academia Sinica, Taipei 106, Taiwan, Department of Applied Chemistry, National Chiao-Tung University, Hsin-Chu 300, Taiwan, and Department of Chemistry and Biochemistry, Florida International University, 11200 SW Eighth Street, Miami, Florida 33199

Received: February 28, 2009; Revised Manuscript Received: April 27, 2009

Ionization and dissociation mechanisms of pyrrolidine in intense 800 nm laser field (10^{13} to 10^{14} W/cm^2) have been experimentally investigated by using a method of molecular beam and time-of-flight mass spectrometer. Singly charged parent ion and numerous fragment ions are observed in the mass spectra, which are investigated as a function of laser intensity and polarization. In order to understand the details of the ionization processes of pyrrolidine in intense femtosecond laser field, we quantitatively calculate the rate constants and ion yields by means of generalized Keldysh−Faisal−Reiss theory, and the excitation probabilities of the excited states are also calculated by using Floquet theory. The results suggest that the ionization might occur partially through the excited states of neutral pyrrolidine. Comparing with linearly polarized (LP) laser field, we observe some enhancement of fragmentation with a circularly polarized (CP) laser field above the saturation threshold intensity which might be explained by the active energies of the pyrrolidine molecular ions are different under CP and LP laser irradiated. To interpret the dissociation patterns of the pyrrolidine ions, we have used the Rice−Ramsperger−Kassel−Marcus theory with the potential surfaces obtained from the ab initio quantum chemical calculations.

I. Introduction

Photoionization and photodissociation processes of atoms and molecules in intense femtosecond (fs) laser fields have been widely studied recently.[1−4] It is well-known that a great number of dynamical phenomena such as high harmonic generation (HHG),[5,6] molecular alignment,[7,8] Coulomb explosion (CE),[9,10] and quantum control of reactions[11] are involved in these processes. However, up to the present, as the basic process, there also exist many ambiguous problems in photoionization and photodissociation mechanisms due to their complexity, especially in the case of molecules. For example, in an intense fs laser field (10^{13} to 10^{14} W/cm^2), if the electric field is not large enough (in other words, the ponderomotive potential is relatively small), the ionization process is considered to be more complicated owing to the competition between multiphoton ionization, tunneling ionization, excitation of excited states, and so on. On the other hand, aside from the laser intensity and wavelength, during the past 20 years, many researches have focused on the polarization effect on the ionization and dissociation processes for molecules from diatomic molecules to large polyatomic molecules.[12−15] Some of the research showed a great attenuated fragmentation of diatomic molecules by using a (CP) laser field resulting from the suppression of rescattered electrons since they are driven away from the parent ion in the CP laser field.[12] However, the enhancement of the fragmentation by the CP laser field has also been observed in some cases, such as anthracene,[16] and whether the direction of the laser field is or is not parallel to that of the induced dipole moment of the cation may influence the ion decomposition, so that the CP laser enhances fragmentation channels. Recently, this phenomenon has also been observed during the ionization and dissociation processes of C_{60} interacting with an elliptically polarized fs laser field.[17]

Pyrrolidine and its derivatives act as the primary functional group on the composition of medicines and also build up a significant proportion of biologically active small organic molecules. By calculating the absorption of the pyrrolidine cation, it should be noted that there is no resonant excited state that exists at 800 nm. Therefore, it is meaningful to investigate the influences of the laser polarizations on the ionization and dissociation of pyrrolidine in an intense fs laser field.

In the previous papers,[18,19] we have reported our studies of intense laser ionization/dissociation of ketones. A main purpose of our studies of intense laser ionization/dissociation of polyatomic molecules is to examine the possibility of employing this technique to be a new type of mass spectrometry. In this paper, we present a comparative study of ionization and dissociation processes of a pyrrolidine molecule with a LP or CP 90 fs, 800 nm laser in the intensity range of 2×10^{13} to 4×10^{14} W/cm^2. The generalized Keldysh−Faisal−Reiss

† Part of the "Hiroshi Masuhara Festschrift".

* To whom correspondence should be addressed. E-mail: dajund@jlu.edu.cn. Tel: +86-431-85168819.

‡ National Taiwan University.

§ Academia Sinica.

|| National Chiao-Tung University.

⊥ Florida International University.

10.1021/jp901857k CCC: $40.75
Published on Web 05/18/2009

(g-KFR) theory, which is successfully used to estimate the ion yields of cyclopentanone in our previous paper[19] and linear alcohols,[20] is chosen to calculate the photoionization rate constants of pyrrolidine. An obvious deviation is found by comparing the results with the experimental measurements. Considering the influence of excitation on the ionization process, this deviation might be attributed to the excitation from the ground state to the electronic excited states followed by further ionization. In addition, some enhancement of fragmentation with CP laser excitation is observed experimentally, which has been attempted to be interpreted by considering different active energies the pyrrolidine cation possessed for CP and LP laser. A qualitative understanding of the femtosecond dissociation of pyrrolidine has also been tried by using Rice−Ramsperger−Kassel−Marcus (RRKM) theory based on the ab initio calculations.

II. Experimental Section

The experimental apparatus used for the fs laser ionization/dissociation study has been described elsewhere.[18,19] Briefly, a chirped pulse amplified (CPA) Ti:sapphire laser (TSA, Spectra-Physics) is employed to produce a 90 fs, linearly polarized laser beam with a repetition rate of 10 Hz and a wavelength centered at 800 nm. The laser polarization can be changed to circular polarization using a quarter-wave plate. Variable attenuation of the beam intensity is achieved using a rotatable half-wave plate followed by a Glan−Taylor prism, which can also ensure that the direction of laser polarization is parallel or perpendicular to the flight axis of the time-of-flight mass spectrometer (TOF−MS) during changes in the beam intensity. The laser beam is focused by a quartz plano-convex lens ($f = 250$ mm) onto a molecular beam of pyrrolidine for providing a laser intensity in the range of 10^{13} to 10^{14} W/cm^2. The molecular beam is generated in a vacuum chamber with a background pressure of 10^{-5} Pa by a pulsed valve with 400 μs duration, and the commercial pyrrolidine sample (ACROS Co. Ltd., 99% purity) is used without further purification. A linear TOF-MS is operated on Wiley−McLaren focusing condition. The produced ions are introduced into a 90 cm field-free region after two-step acceleration and finally are detected by a dual microchannel plate (MCP) detector. A slit with 0.5 mm width is mounted in front of the flight tube to ensure that only the ions produced in the center portion of the laser focus volume can enter the drift tube. The mass spectra are obtained, accumulated, and averaged by connecting the ion detector output through a fast preamplifier to a digital storage oscilloscope (Tektronix TDS 3054B) and then transferred into a computer. Typically the mass resolution $m/\Delta m$ at $m/e = 100$ is about 1000. Ion intensities (corresponding to ion yields) are evaluated by integrating the ion signals for the mass peak in the spectrum.

III. Results

A. Intensity Modification of the CP Laser Field. Even if the polarization of the laser is different, the saturation intensity of the singly charged pyrrolidine ion should be the same in the case where we take the equivalent laser electric field (the peak amplitude of the laser electric field is the same for both polarizations) into account.[21] In other words, if the laser intensity for CP is multiplied by some factor, the saturation intensity of the pyrrolidine parent ion is the same as that of LP. This conclusion has been derived on the basis of Ammosov−Delone−Krainov (ADK) theory[22] and identified experimentally by using intense femtosecond laser irradiation for Xe.[23] It is predicted that the laser intensity I for CP is 1.3 times higher than that for LP within the framework of ADK theory. For a given laser intensity, if the peak amplitude of the electric field for LP is E_0, then that for equivalent CP will be $E_0/\sqrt{2}$. Thus, in order to obtain the same ion yield, the laser intensity of the CP should be multiplied by a factor of 0.65.[16,23]

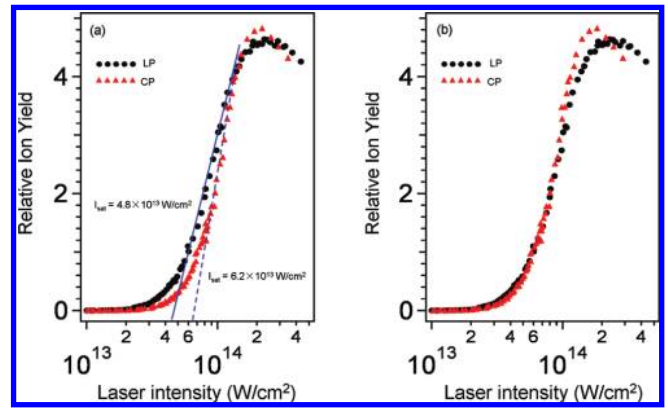

Figure 1. Singly charged pyrrolidine ion yields vs laser intensities for LP and CP on a log-linear plot. (a) The ion yields are plotted as a function of experimentally measured laser intensity for both polarizations. From the figure, the I_{sat} of pyrrolidine is estimated. $I_{sat} = 4.8 \times 10^{13}$ W/cm^2 for LP, whereas $I_{sat} = 6.2 \times 10^{13}$ W/cm^2 for CP. (b) The horizontal axis for CP is shifted by a factor of 0.77 in order to ensure the saturation intensities are the same for both polarizations.

In the present work, Figure 1 shows the ion yields of singly charged pyrrolidine ion produced by LP and CP, respectively. It can be seen from Figure 1a that the saturation intensity I_{sat} is 4.8×10^{13} W/cm^2 for LP and 6.2×10^{13} W/cm^2 for CP. As mentioned above, we adjust the horizontal axis for CP by a factor of 0.77 in Figure 1b. This shift insures the saturation intensities for both polarizations are the same, and this factor is acceptable by comparing with the theoretical prediction (0.65). Therefore, in the following, we will use this modified intensity for discussions.

B. TOF−MS Observations of Pyrrolidine by Both Polarizations. The mass spectra of pyrrolidine for LP and CP laser fields at different intensities are illustrated in Figure 2. At the laser intensity $I = 4.5 \times 10^{13}$ W/cm^2 (nearby the saturation intensity $\sim 5 \times 10^{13}$ W/cm^2, in panels a and b of Figure 2), the mass spectra for both polarizations exhibit similar patterns with a dominant peak from the singly charged parent ion and some weak peaks from the fragment ions. This polarization independence characteristic in a relative low intensity region has been observed on benzene by Chin and co-workers previously.[24] At the laser intensity $I = 1.5 \times 10^{14}$ W/cm^2 (above the saturation intensity, in panels c and d in Figure 2), the fragment ions are more abundant for both polarizations. By comparison, it looks like the ion yields of fragment ions are more or less higher for the CP laser field at this intensity. Some relative small fragment ions, such as ions with $m/z = 30$, 15, and 1, exhibit some enhancement as well. Furthermore, when the laser intensity is up to 4×10^{14} W/cm^2, the doubly charged parent ions can be observed although it is quite small and the results are not shown in this paper.

For comparison, an electron impact ionization mass spectrum[25] is also listed in Figure 2e. We can easily see that the relative peak intensities of the fragments are different from our experimental results due to the fact that the energies deposited into the parent ions are somehow different among both experimental conditions, which leads to the difference of rate constants for ions decomposition.

The intensities of the parent ion and a fragment ion, $m/z = 43$, as a function of laser intensity from 2×10^{13} to 4×10^{14} W/cm^2

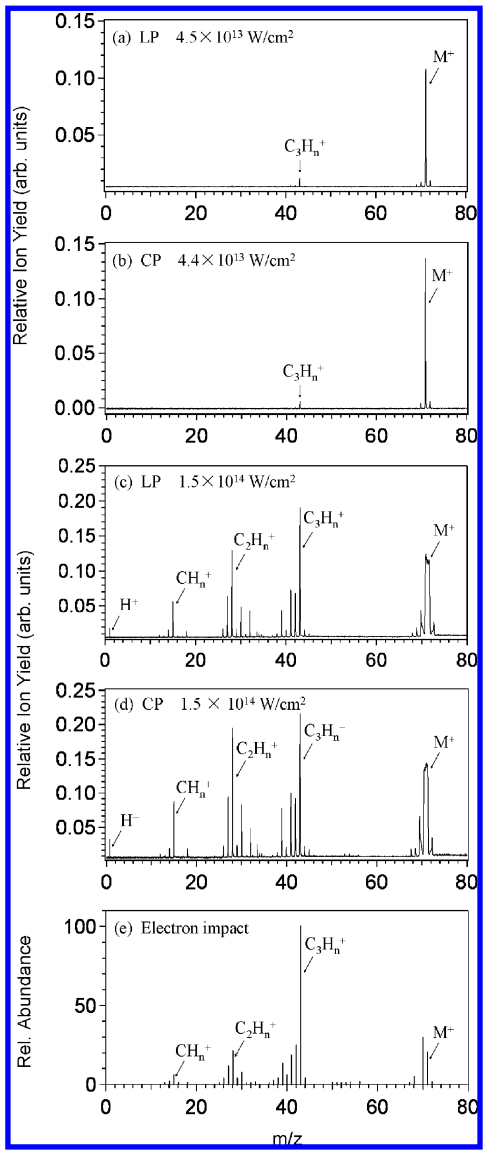

Figure 2. TOF−MS of pyrrolidine obtained by LP (a and c) and CP (b and d) laser fields as well as the MS provided by electronic impact technique[25] (e). The presented laser intensities are scaled.

are plotted with log−log form in Figure 3, panels a and b, for LP and CP laser fields, respectively. Here the ion intensities are determined from the ion peak area below the curves in the measured mass spectrum. Because the absorbed energy for ionization has to be beyond the ionization potential energy of the pyrrolidine molecule (8.77 eV[25]) in a multiphoton ionization (MPI) regime, six laser photons are required to be absorbed. However, the laser intensity dependences of the measured parent ion yields for both polarizations roughly show a power law $\sim I^4$, that is, the slope of 4 in log−log scale which is significantly lower than the number of the photons required for ionizing the molecules. This may indicate that the ionization process consists of two sequential processes, one of which is the excitation process which is characterized by an $\sim I^4$ dependence, the other one is the ionization from the excited state. Due to the influence of the rate-determining step on photoionization process, the parent ion yields show a behavior of $\sim I^4$.

IV. Theoretical Treatments of Intense Laser Ionization and Excitation

Several theoretical methods have been used to treat for ionization processes of polyatomic molecules, such as ADK,[22,26,27] Keldysh,[28−30]

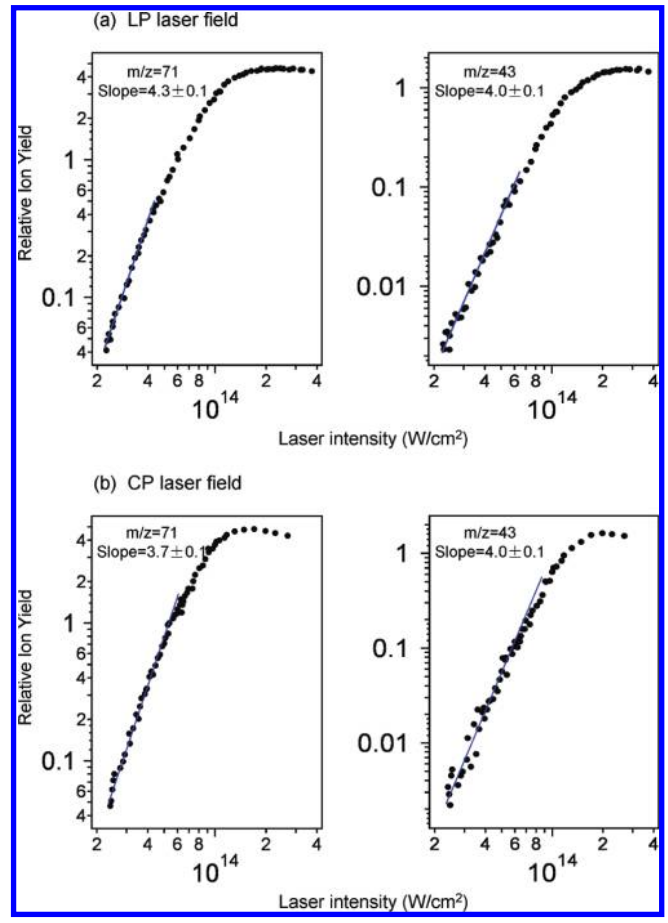

Figure 3. Relative ion yields of parent and main fragment ion as a function of laser intensity: (a) LP and (b) CP. The wavelength is 800 nm. A linear fit through the data points is shown as the solid line.

and KFR theory,[28,31,32] in various studies. In the present work, in order to calculate the ionization rate constant of a pyrrolidine molecule, we use a g-KFR theory which is a generalization of the original KFR theory to molecules.[6] For comparison with the experimental results, we combine the calculated rate constants with the rate equations to calculate the ion yields.

On the other hand, some studies have discussed the possibilities of electronic excitation by an intense laser.[33,34] It might be considered that the behavior of the excitation process plays an important role for the ionization process but the continuum state above the ionization threshold is not included in this work of collective excitation processes.[34] Accordingly, in this work we also study how the ion yields will behave as a function of laser intensity when the collective excitation processes take place.

A. Theoretical Model for the Ionization Processes. The g-KFR theory[6] is developed from the theory originally proposed by Faisal[35] based on the Keldysh theory for hydrogen atom and developed with the S-matrix formalism by Reiss.[36] Later by combining the molecular orbital (MO) theory and the Born−Oppenheimer (BO) approximation, the KFR theory is generalized to molecules (g-KFR) which has been described elsewhere.[19,37] Briefly, in g-KFR theory it is assumed that the ground electronic state of a molecule (or its cation) is well described in terms of molecular orbitals and obtained from ab initio calculation. For the ionized state, the ionized electron wave function is described by the Volkov continuum state.

Under the assumption that the ionization only takes place from the highest occupied molecular orbital (HOMO), the photoionization rate constant can be formulated as

$$k(\vec{F}) = \sum_{N>(I_0+c_\xi^2 U)/\omega}^{\infty} k_N \tag{4-1a}$$

with

$$k_N = 2\pi S^2 \sum_{j,j'=1}^{N_a} c_j c_{j'}^* \int \frac{d^3p}{(2\pi)^3} \hat{\chi}_j(\vec{p}) \hat{\chi}_{j'}^*(\vec{p}) \left(\frac{p^2}{2m_e} + I_0\right)^2 \times \left| J_N\left(c_\xi V_p, c_\xi^2 \frac{U\cos\xi}{2\hbar\omega}, \alpha\right)\right|^2 \cos(\vec{p}(\vec{R}_j - \vec{R}_{j'})) \delta\left(I_0 + c_\xi^2 U + \frac{p^2}{2m_e} - N\omega\right) \tag{4-1b}$$

where

$$V_p = \frac{eF}{m\omega^2\hbar}\sqrt{(p_x\cos(\xi/2))^2 + (p_x\sin(\xi/2))^2},$$

$$\alpha = \tan^{-1}\left(\frac{p_y}{p_x}\tan\frac{\xi}{2}\right), \quad \xi = 0\left(\xi = \frac{\pi}{2}\right)$$

corresponds to LP (CP) laser field, $c_\xi = 1$ ($c_\xi = \sqrt{2}$) for $\xi = 0$ ($\xi = \pi/2$), N_a is the number of atoms in a molecule and $U = (eF)^2/(4m_e\omega^2)$ is the ponderomotive potential associated with the optical field of frequency ω. In eq 4-1b $\hat{\chi}_j$ is the Fourier transformed atomic orbital of atom j, $\vec{R}_j$ is the coordinate of atom, $J_N(a,b,\alpha)$ is a generalized Bessel function with three arguments, c_j denotes the coefficients of the linear combination of atomic orbitals-molecular orbital (LCAO-MO), I_0 is the ionization potential of molecule, $S = \sqrt{2}$ for the closed shell parent molecule or molecular cation, and $S = 1$ for the open shell case.

A detailed derivation and discussion of $k(\vec{F})$ is explained in the original paper.[37] For multi-ionization of molecules, we consider the following sequential ionization process

$$M \xrightarrow{k_1} M^+ \xrightarrow{k_2} M^{2+} \cdots \xrightarrow{k_n} M^{n+} \tag{4-2}$$

where k_i is the photoionization rate constant of the M^{i+} cation.

B. Theoretical Model for Excitation Processes. The collective excitation is defined in a way that excited state probabilities as a function of laser intensity behave in the same manner $\sim I^n$ during the multiphoton region.[34] Here we give formalisms of the Floquet method[38] to show how the electronic excited states will populate by these mixings. By applying the Floquet method, we can solve the periodically time-dependent Schrödinger equation

$$\left(\hat{H}(r,t) - i\frac{\partial}{\partial t}\right)\phi(r,t) = 0 \tag{4-3}$$

with the total Hamiltonian

$$\hat{H}(r,t) = \hat{H}_0(r,t) + \hat{V}(r,t) \tag{4-4}$$

where $\hat{V}(r,t)$ is the time periodic interaction Hamiltonian $\hat{V}(r,t + T) = \hat{V}(r,t)$ between the system and a laser field.

The quasistate wave function is given in a series of Fourier expansions

$$\phi_\alpha(r,t) = \exp(-i\varepsilon_\alpha t)\sum_{n=-\infty}^{\infty} A_\alpha^{(n)}(r)\exp(-in\omega t) \tag{4-5}$$

with $A_\alpha^{(n)}(r) = \sum_\beta \chi_{\alpha\beta}^{(n)}(r)|\beta\rangle$. Thus by putting eq 4-5 into the Schrödinger equation, we obtain the following coupled equation:

$$\sum_{n,\beta}[\langle\alpha|\hat{H}^{(n-m)}|\beta\rangle - (\varepsilon_\alpha + n\omega)\delta_{nm}\delta_{\alpha\beta}]\chi_{\alpha\beta}^{(n)}(r) = 0 \tag{4-6}$$

with $\hat{H}^{(n)} \equiv {}^1/_T\int_0^T \mathrm{d}t\, \hat{H}(r,t)\exp(in\omega t)$ which is nonzero only for $n = 0, \pm 1$. Equation 4-6 is equivalent to diagonalize the following matrix $\tilde{E}$:

$$(\tilde{E})_{NM} = (E_\alpha - n\omega)\delta_{\alpha\beta}\delta_{nm} + V_{\alpha\beta}\delta_{n\pm1,m} \tag{4-7}$$

where $N = (n + n_s)(N_s + 1) + \alpha + 1$, $M = (m + n_s)(N_s + 1) + \beta + 1$, $n,m = -n_s, ..., n_s$, $\alpha,\beta = 0, ..., N_s$ and $(V)_{\alpha\beta} = \langle\alpha|\hat{V}^{(\pm1)}|\beta\rangle$. n_s is infinite in principle; however, in the actual numerical calculation, we use a finite number of photon numbers. By defining the obtained eigen energies and eigen vectors as ε_j and ϕ_j, the time-dependent molecular ion wave function can be written as

$$\Phi(t) = \sum_j \langle\phi_j|\phi_0^0\rangle\exp(-i\varepsilon_j t)\phi_j \tag{4-8}$$

where $(\psi_i^n)_N = \delta_{N,n(N_s+1)+i+1}$ for $N = 1, ..., (2n_s+1)(N_s+1)$ and $n = -n_s, ..., n_s$. The population of the ground ($i = 0$) and excited states ($i = 1, ..., N_s$) are calculated as

$$|C_i(t)|^2 = \sum_{n=-n_s}^{n_s} |\langle\psi_i^n|\Phi(t)\rangle|^2 \tag{4-9}$$

V. Discussion

A. Ionization Processes of Pyrrolidine in Different Polarized fs Laser Fields. Acting as a qualitative criterion for the ionization processes, the Keldysh parameter[28,39] γ is defined by

$$\gamma = \left(\frac{I_0}{1.87\times10^{-13} I\lambda^2}\right)^{1/2} \tag{5-1}$$

where I_0 is the ionization potential energy, I is the laser intensity, and λ is the laser wavelength. If $\gamma \gg 1$, the MPI is dominant. In present work, the value of the Keldysh parameter tends to 1 when the laser intensity is around 7.1×10^{13} W/cm^2. Moreover, from Figure 3 it should be noted that we discuss the order of the laser dependence below 5×10^{13} W/cm^2. In other words, when a 800 nm fs laser irradiates the pyrrolidine molecules, it should be evident that MPI play a significant role if the laser intensity is lower than the saturation intensity.

In order to quantitatively understand the ionization processes of pyrrolidine in intense fs laser field, the hydrogen-like atom model and the g-KFR theory are used for the calculation of rate constants of ionization processes where the excitation

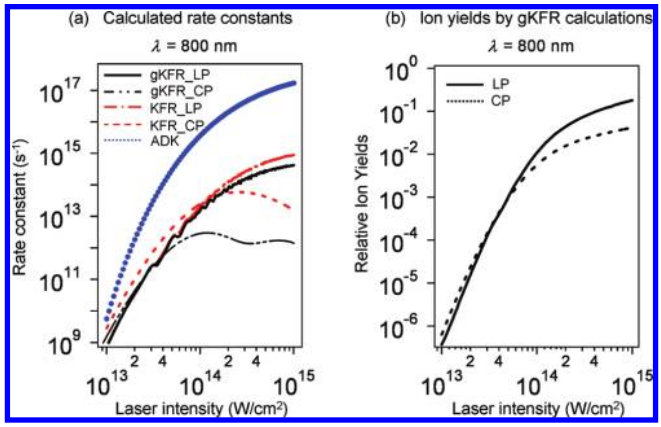

Figure 4. (a) Ionization rate constants of the neutral pyrrolidine molecule are plotted as a function of laser intensity by using the KFR (hydrogen-like atom calculation) (red lines), generalized g-KFR (black lines), and ADK (blue dots) theories. (b) Laser dependence of ionization yields of the pyrrolidine molecular cation calculated by the g-KFR theory for the LP and CP laser are plotted as a solid and dotted lines, respectively. The slopes of both plots are approximately estimated as 5∼5.2. The pulse duration of laser is 90 fs for the LP and CP lasers.

processes during ionization processes are neglected. In the following calculation, we choose the 800 nm laser wavelength used in the experiment and the value of the ionization potential of pyrrolidine molecule provided by NIST[25] (I_0 = 8.77 eV). For a hydrogen-like atom calculation, a molecule is regarded as a hydrogen atom with one electron where the atomic orbital is 2p, whereas for the molecule case, a realistic HOMO has been used in which the 2p orbital is mixed with a 3p orbital. The HOMO and geometry optimization for the pyrrolidine molecule are performed using the quantum chemical calculation by the DFT-B3LYP method with the basis set 6-31+G**, and all these calculation results are obtained by using the Gaussian 03 program.[40]

In Figure 4a the ionization rate constants of a neutral pyrrolidine molecule are plotted as a function of laser intensity by using the KFR (red lines), g-KFR (black lines), and ADK (blue dots) theories. As mentioned above, the KFR and ADK theories are applied for the hydrogen-like atom, whereas the g-KFR is used for the pyrrolidine molecule. Actually, the ADK theory is well-known to consider only the static laser field; on the other hand, the KFR and g-KFR theories can deal with the LP and CP lasers. For calculation by the KFR theory, CP and LP lasers are used. From the figure we find that the result from the ADK theory overestimates the rate constant obviously. By comparing the results of the KFR and g-KFR theories, it is found that independently of LP or CP laser, the result of g-KFR theories are somehow smaller than those obtained from the KFR, and difference is within 10^1 order for LP laser whereas within 10^2 order for CP laser. Difference between KFR and g-KFR calculations will be increased for larger intensity, especially for $I > 10^{14}$ W/cm^2.

Figure 4b illustrates the laser dependence of the yields of the singly charged pyrrolidine molecular ion calculated by the g-KFR for both LP and CP lasers. It should be noted that the ion yield calculated for the CP laser is larger than that for the LP laser below 4×10^{13} W/cm^2. In contrast, the ion yield for the LP laser will overcome that for the CP laser beyond the above laser intensity region, and the difference reaches a factor of about 5 at 10^{15} W/cm^2. This results is consistent with the results of the Xe ion yields in CP and LP lasers where they use a different definition of laser electric field in the CP laser.[17] As can be seen from Figure 4b, the slopes for both LP and CP lasers predicted by g-KFR theory can be approximately estimated as 5.0∼5.2, which are somehow different from our experimental measurements (∼4.0). Although g-KFR theory is successful in predicting the ion yield of cyclopentanone, in this work it cannot completely explain the ionization process of pyrrolidine in 90 fs laser field. Below the saturation intensity the parent ion yield roughly follows a power law of I^4, which implies that the excited states should take part in the ionization process which is totally neglected in g-KFR calculations.

Whereafter, in the interest of understanding the influence of the molecular excited states on the ionization process, we first calculate the absorption spectrum of the neutral pyrrolidine molecule in terms of the time-dependent density functional theory (TDDFT) method as described in our previous study for cycloketones.[18] Briefly, the optimized geometric structure of the neutral pyrrolidine molecule is determined by a DFT calculation of the B3LYP method with 6-31++G** basis set, and then a TDDFT of UB3LYP method with the same basis set is used to calculate the transition energies and the oscillator strengths between the ground and excited states based on the molecular structure obtained. Finally, the optical absorption spectrum shown in Figure 5a is drawn from these calculated results with the help of the SWizard program.[41] This calculated result is compared with that provided by Pickett et al.[42] by means of a fluorite prism vacuum spectrograph and a Beckman spectrophotometer. It may be noted that the calculated local maximum in the absorption spectrum is shifted to the blue region by approximately 10 nm. From Figure 5a, a considerably strong

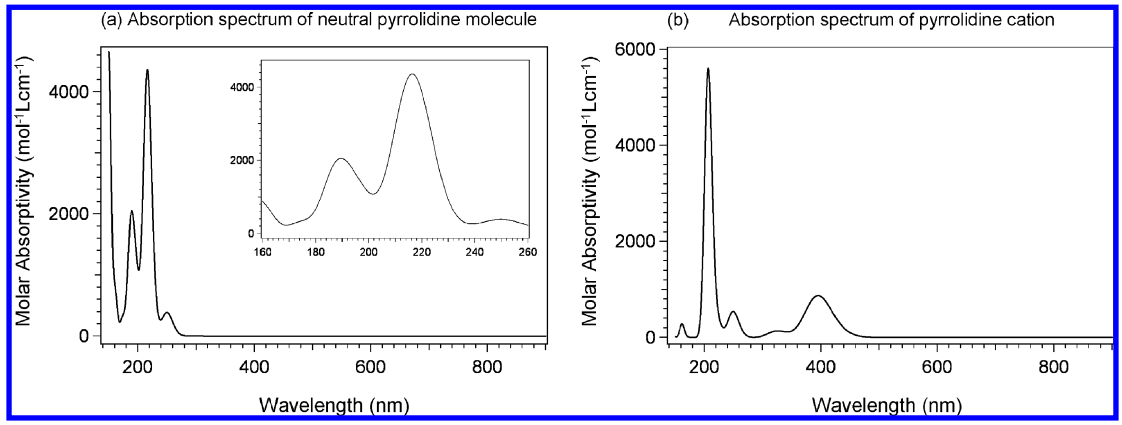

Figure 5. Calculated absorption spectra of the neutral pyrrolidine molecule (a) and singly charged pyrrolidine cation (b) by using the Gaussian 03 program. The inset figure shows the spectral characteristic from 160 to 260 nm.

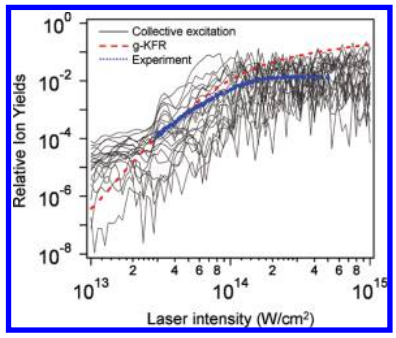

Figure 6. Comparison of the parent ion yields that predicted using both collective excitation model (gray lines, including 30 excited states of the pyrrolidine molecule) and g-KFR theory (red broken line) with that measured by experiment (blue dots). The pulse duration of laser is 90 fs.

absorption band exists near 200 nm with a weak maximum at approximately 220 nm. From the view of absorbed energy, it corresponds to 4-photon absorption in our present work. Accordingly, in the multiphoton process, a resonant excitation from the ground state to the excited state of the neutral pyrrolidine molecule followed by further ionization reaching to the continuum state might be a possible ionization channel, which represents a power order of $\sim I^4$.

In addition, the theoretical analyses show that the neutral pyrrolidine molecule undergoes a collective excitation followed by further ionization, it might be another possible ionization channel which also shows a $\sim I^4$ behavior. Within this framework, we apply the Floquet theory to explore how the probabilities of excited states of the neutral pyrrolidine molecule will behave as a function of laser intensity instead of directly seeing the behavior of the ionization. Total 30 excited states of neutral pyrrolidine included in calculation are obtained by CIS method with the basis sets 6-31+G**. The quantum chemical calculations predict that the energy of the first excited state of this molecule is 6.89 eV and the largest energy among excited states is 11.59 eV. The results are illustrated in Figure 6 with log−log scale (gray lines). As can be easily seen from the figure, all excited states roughly exhibit a similar behavior; that means the slopes are almost independent of the energy of the excited states. These slopes can be approximately estimated as 4∼5.

We also compare the experimental measurements with both theoretical predictions in Figure 6. Just as the descriptions mentioned above, from this figure we can immediately see that the slope of the laser dependence of the yield of the pyrrolidine cation predicted by g-KFR theory is larger than that obtained by experiment, whereas the collective excitation process shows relatively better agreement with the experimental results. Therefore, it might be expected that the ionization process through excite states can decrease the slope of the ion yields.

B. Enhancement of the Fragmentation by CP Laser Field. Actually, we consider that the ionization is followed by dissociation, since for neutral dissociation of a molecule to take place, the molecule has to absorb energy from the laser first and then the molecule will either predissociate or decompose after internal conversion. The decomposed products then ionize afterward, and all these steps have to take place within the laser pulse duration of ∼100 fs, making this scenario rather unlikely.[34] As can be seen from Figure 2, the fragmentation of the pyrrolidine irradiated by different polarized 90 fs laser fields at 800 nm are not heavy even at high intensity. Since no available pyrrolidine cation absorption spectra can be found, we also simulate it by using the method as mentioned above, the calculation result is shown in Figure 5b. Similar to the neutral

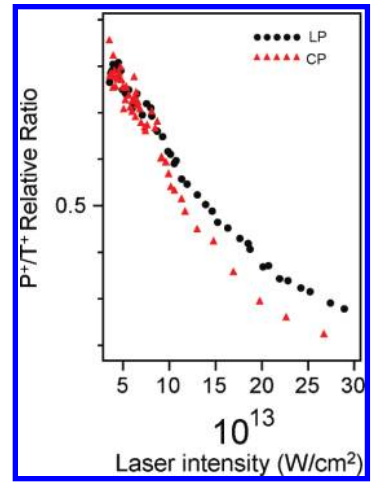

Figure 7. Ratio of the parent ion yield P^+ to the total ion yield T^+, P^+/T^+ is plotted as a function of the laser intensity.

pyrrolidine molecule, the absorption spectrum of singly charged pyrrolidine ion also has no single photon absorption nearby 800 nm but with a strong absorption band around 400 nm. On account of the importance of resonance between the excitation wavelength and the electronic energy levels, this absence of the single photon resonance at 800 nm can be taken as an evidence for illustrating the weak fragmentation of pyrrolidine observed.

Now we will study the polarization effects under this nonresonant condition (800 nm). From Figure 2 the fragmentation of pyrrolidine is somewhat enhanced with increasing the laser intensity in the CP laser field, especially above the saturated intensity. As shown in Figure 7, the ratio of parent ion yield P^+ to the total ion yield T^+, P^+/T^+, for CP is decreased drastically with increasing the laser intensity compared with that for the LP case, which might imply that the active energies of the pyrrolidine cation are different for both polarizations before the dissociations take place and the CP laser favors further fragmentation. Considering the complexity of the ionization and dissociation processes involved, the difference in active energies should be attributed to several reasons, and now we attempt to present some possibilities.

According to the g-KFR theory mentioned above, we could qualitatively understand that the Volkov state which is used to describe the ionized state is as a function of the laser field. It means that, with increasing the laser intensity, the Volkov function could behave differently for CP and LP laser fields, leading to the active energies difference. Moreover, when we discuss the dissociation of the pyrrolidine ions by different polarizations, the direction characteristics of the laser fields should be taken into account. As Nakashima et al. pointed out,[16] if the direction of the laser polarization is parallel or nearly parallel to the direction of the induced dipole moment, the initial resonance excitation of molecular cation fragmentation may be achieved. Compared with the LP laser, the CP laser can be interacted with a larger part of randomly oriented molecules and leads to the production of more fragments. This aspect should be another possible reason resulting in the difference of active energies for both polarizations.

Besides, for the purpose of discussing the mechanism of enhancement of molecular ion fragmentation in the CP laser field quantitatively, we also calculate the total summation of excitation probabilities of the excited states for the pyrrolidine cation in CP and LP lasers by Floquet theory as shown in Figure 8. The number of excited states is chosen as 100, and the excited

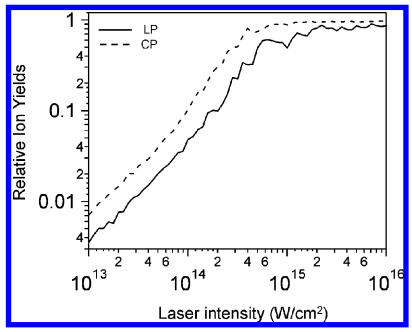

Figure 8. Excitation probabilities of the summation of 100 excited states of the pyrrolidine cation for both CP and LP lasers.

states of the molecular ion are calculated as similarly done in the neutral pyrrolidine molecule. The results show that for the laser intensity $I > 10^{13}$ W/cm^2 the probability is mostly larger in CP laser, and the difference between CP and LP lasers depends on the laser intensity. This fact seems to be consistent with the enhancement of molecular ion fragmentation in the CP laser field, and it is also expected that the different excitation probabilities for both polarizations will somehow affect the patterns of molecular ion fragmentation.

However, it should be emphasized that the laser intensities (2×10^{13} to 4×10^{14} W/cm^2) we used in the present work still do not reach the intensity at which rescattering takes place ($\sim 10^{15}$ W/cm^2). Therefore, the electron rescattering model,[43,44] in which more fragmentation will be produced in the LP laser, is not used for interpreting the difference of the fragmentation for different polarizations yet.

C. Ab Initio/RRKM Calculations of the Dissociation Mechanism. Ionization of molecules in intense laser field is usually accompanied by absorption of additional excess energy by molecules, which is sufficient for secondary isomerization and fragmentation processes. Secondary reactions can occur either in an excited state of the ion or in the ground state after relaxation through internal conversion or intersystem crossing. Great variation in the energy that can be absorbed by each molecule in an intense laser field can lead to the existence of different dissociation processes taking place simultaneously. So the final mass spectrum can be a superposition of several dissociation reactions occurring in different electronic states. Internal conversion into the ground electronic state can be strongly facilitated by conical intersections between the excited and the ground states. For example, it was reported recently[45] that the S_1 state of triazine ($C_3H_3N_3$) has a conical intersection with the ground state at an open chain structure. Relaxation to the ground state in the open chain geometry initiates dissociation reactions with branching ratios of products different from those from the cyclic intermediate. An ab initio and experimental study of the dissociation of cyclopentanone (C_5H_8O) in an intense laser field[19] revealed that the first excited state of the cation has a conical intersection with the ground state at an opened chain structure, which provides internal conversion from the D_1 to D_0 state and determines the ensuing dissociation processes. The structure of pyrrolidine is similar to that of cyclopentanone that led us to assume that dissociation reactions of the pyrrolidine cation can be similar to that of cyclopentanone.

To study the dissociation mechanism of the pyrrolidine cation, we performed ab initio quantum chemical calculations of potential energy surfaces (PES) for $C_4H_9N^+$. The B3LYP/6-31G* method[46,47] has been used to carry out geometry optimizations and the energies of the ions have been refined by the G3(MP2,CCSD) ab initio calculations.[48,49] The zero-point energy

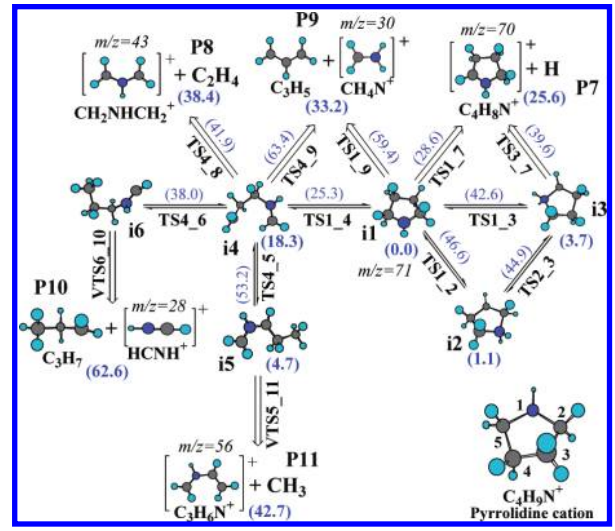

Figure 9. Simplified dissociation scheme of pyrrolidine cation in the ground electronic state.

corrections to the total G3(MP2,CCSD) energies have been computed using B3LYP/6-31G* frequencies without scaling. All ab initio calculations have been performed using the Gaussian 03[40] and MOLPRO 2002 packages.[50] B3LYP/6-31G* frequencies for all intermediates and transition states have been used to perform the RRKM calculation.[51] Qualitative calculations of D_1 and D_2 excited state PESs of the pyrrolidine cation were performed at the CASSCF(11,11)/6-31G* level.

D. Ground State Dissociation of the Pyrrolidine Cation. The complete dissociation scheme of the pyrrolidine cation is very complicated due to a great variety of possible reaction channels. Fortunately, the PES can be subdivided into several independent parts separated by relatively high barriers. Dissociation branching ratios mostly depend on the reaction channels in the vicinity of the initial intermediate and weakly influenced by reactions from other parts of PES. Therefore we do not present all dissociation channels and concentrate only on the part of PES, which is the most interesting for our discussion.

A simplified dissociation scheme of the pyrrolidine cation with geometry closed to the parent pyrrolidine molecule is presented in Figure 9. Intermediate **i1** is a cyclic isomer corresponding to the structure of the parent pyrrolidine molecule, whereas isomers **i2** and **i3** are produced from the parent molecule by a hydrogen shift. Isomer **i4** is formed by ring opening between atoms 2 and 3 in **i1**. This ring-opening occurs through a low barrier of 25.3 kcal/mol (**TS1_4**), whereas the H atom shifts **i1** → **i2** and **i1** → **i3** require much higher barriers, which make any reactions via **i2** and **i3** negligible. H atom elimination **i1** → **TS1_7** → **i7** has a relatively low barrier of 28.6 kcal/mol. We did not find other reactions with low barriers, which can compete with **i1** → **i4** and **i1** → **i7**. Preliminary RRKM calculations reveal that total branching ratios of all other reaction pathways are less than 5% for the entire energy range, and hence, we omitted these minor reactions from the reaction scheme.

The branching ratios of pyrrolidine cation dissociation initiating from intermediate **i1** are given in Figure 10a. The main dissociation channel (near 70%) in the whole energy range is the H atom elimination from position 2 of the ring. The next reaction is $C_4H_9N^+ \rightarrow CH_2NHCH_2^+$ ($m/z = 43$) + C_2H_4. The relative yield of this channel reaches a maximum value of approximately 30% at the available internal energy of 125 kcal/

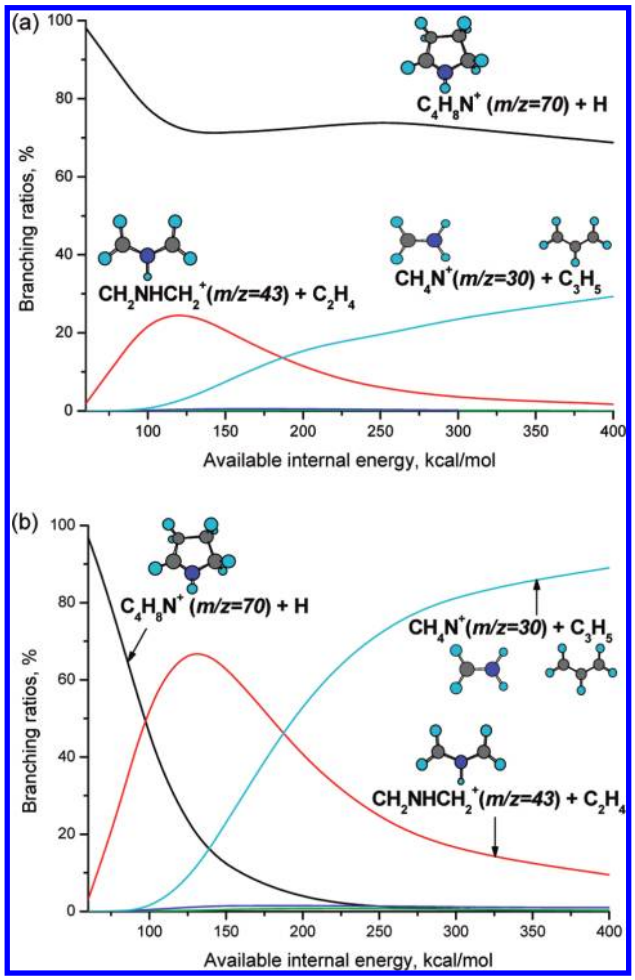

Figure 10. Branching ratios of pyrrolidine cation dissociation: (a) reaction initiates from isomer **i1**; (b) reaction initiates from ring-opening isomer **i4**.

mol and then going down with increasing energy. The branching ratio of the last important fragment CH_4N^+ (m/z = 30) continuously grows with the energy increase, rendering this channel the second most significant at high energies. According to the experimental mass spectrum (Figure 2), the intensity of the H loss reaction must be very low. Even if it is supposed that some of the $C_4H_8N^+$ (m/z = 70) fragments undergo secondary dissociations, the amount of unreacted $C_4H_8N^+$ fragments should be still high at low laser intensity. Moreover, no reactions with low barriers were found for this fragment. Lines with m/z = 1, 15, 27, 28, 39, 41, and 42 can be a result of secondary fragments cracking. However, the intensity of the $CH_2NHCH_2^+$ (m/z = 43) fragment, which is the main candidate for these secondary reactions, decreases rapidly with growing energy. It can be seen from Figure 2 that the parent ion is dominant with little fragments at low intensity. In these fragments, however, the peak with m/z = 43 is the most abundant one. By increasing the laser intensity, this fragment changes to the predominant product in the mass spectra. This trend and the branching ratio between the m/z = 43 and other fragments are all different from the prediction of the RRKM calculation based on the assumption that the fragmentation start from the ground state of the pyrrolidine cation. So we can conclude that dissociation of intermediate **i1** from the ground state geometry cannot explain the experimental mass spectrum (Figure 2) and can add only a minor contribution to the overall dissociation process.

E. Dissociation of the Pyrrolidine Cation Initiated from Excited States. A quantitative diagram of two lowest excited state PESs of the pyrrolidine cation calculated by CASSCF is presented in Figure 11. The cyclic structure, which is a minimum on the ground state PES, is not a local minimum in the D_1 state. Excitation to the D_1 state results in breaking the C_1-C_2 bond and geometry relaxation into the open chain structure similar to **i4**. A small energy gap between D_0 and D_1 at this geometry allows us to suppose an existence of a conical intersection between these terms in a vicinity of this structure enhancing internal conversion from D_1 to D_0 into the open chain intermediate **i4**. The optimized D_2 state has a cyclic structure (Figure 11) with a small energy gap between D_1 and D_2 states and a large energy gap between D_0 and D_1 and D_0 and D_2 states. A small energy gap between D_1 and D_2 at this geometry allows us to suppose the existence of a conical intersection between these terms enhancing internal conversion from D_2 to D_1 followed by relaxation processes on D_1 PES, in particularly by internal conversion to D_0 into the intermediate **i4**.

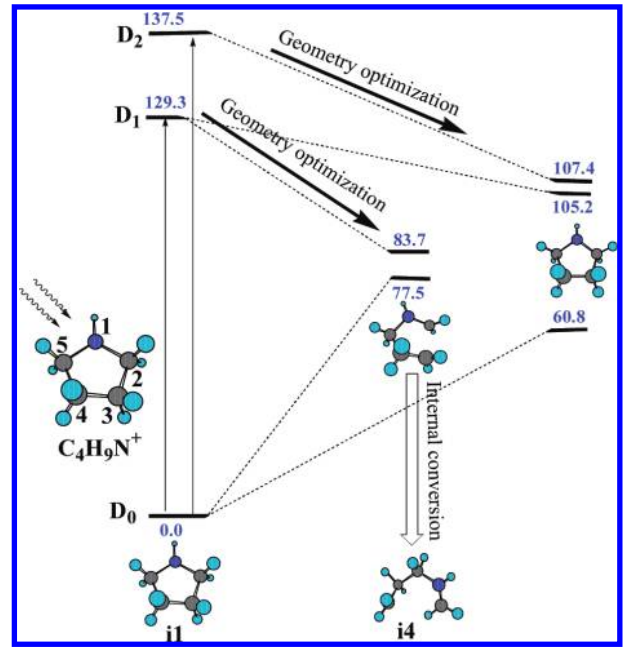

Figure 11. Relaxation mechanism of $C_4H_9N^+$ from the first and the second excited electronic states.

Branching ratios of dissociation products, if the reaction starts from intermediate **i4** after the internal conversion from D_1 state, is given in Figure 10b. The most important dissociation reactions in this case are $C_4H_9N^+ \rightarrow CH_2NHCH_2^+$ (m/z = 43) + C_2H_4 and $C_4H_9N^+ \rightarrow CH_4N^+$ (m/z = 30) + C_3H_5. The intensity of $CH_2NHCH_2^+$ fragment reaches a maximum value at the medium energy region and then going down, whereas the intensity of CH_4N^+ fragment is growing up with increasing the energy. The H atom elimination reaction is important only in low energy region. Comparing the distributions in Figures 10a and b, we can conclude that the second mechanism, through the excitation of pyrrolidine cation to D_1 state followed by internal conversion to D_0 state into **i4** intermediate explain the dissociative ionization process of pyrrolidine in intense fs laser field better than the first mechanism, through the ground state dissociation of cyclic cation. Low intensity of m/z = 70 line in the experimental mass spectrum could be explained either by the small amount of ionized pyrrolidine molecules, which have low internal energy, or by a nonstatistical character of dissociation process that can increase the probability of reaction $C_4H_9N^+ \rightarrow CH_2NHCH_2^+ + C_2H_4$ in comparison with the RRKM calculations.

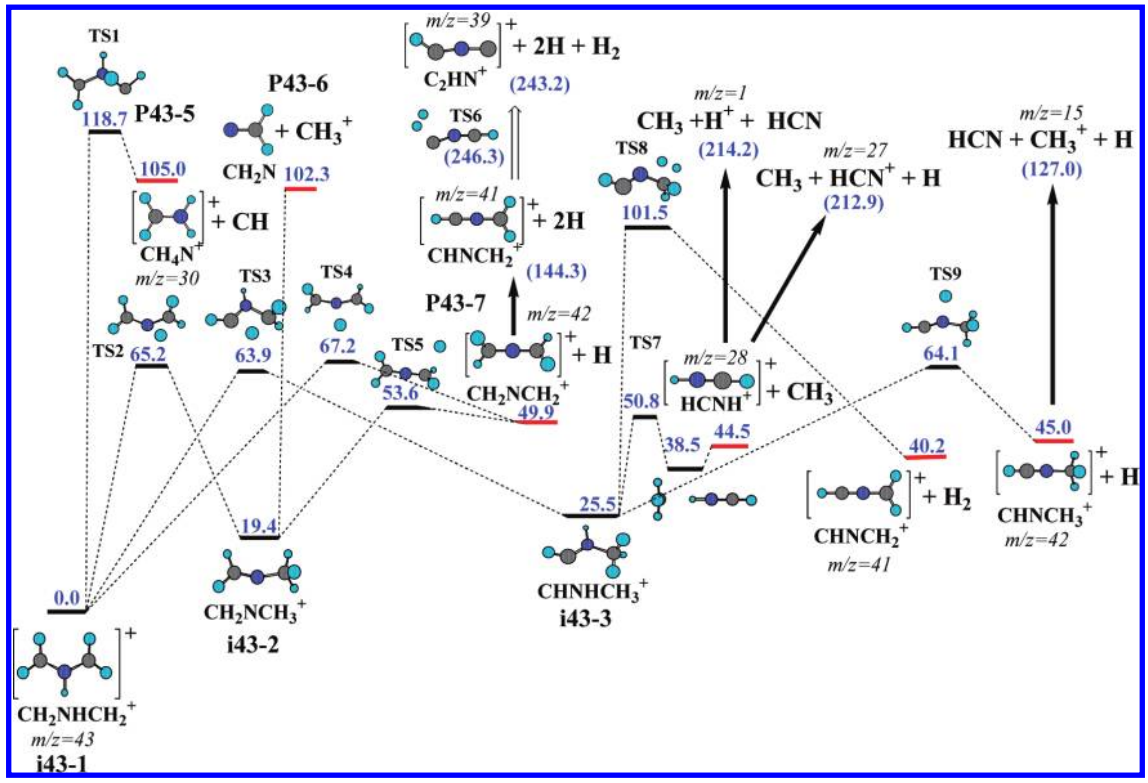

Figure 12. Dissociation of $CH_2NHCH_2^+$ (m/z = 43).

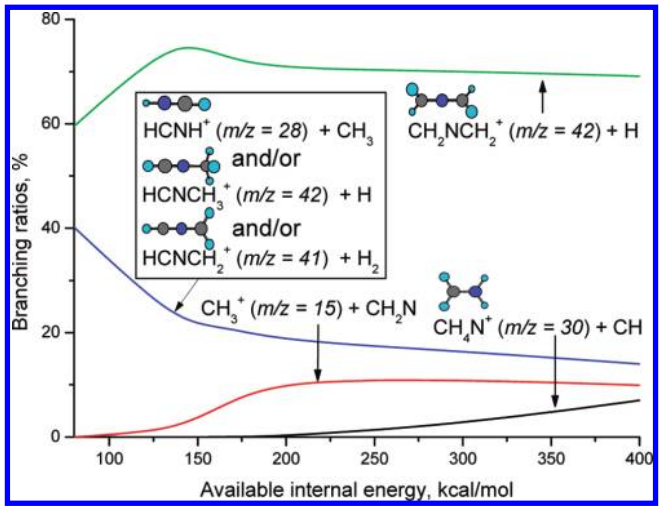

Figure 13. Branching ratios of $CH_2NHCH_2^+$ (m/z = 43) dissociation.

F. Dissociation of Fragment $CH_2NHCH_2^+$ (m/z = 43). The PES of the $CH_2NHCH_2^+$ fragment and branching ratios of dissociation products are given in Figures 12 and 13. Fragment $CH_2NCH_2^+$ (m/z = 42) can be produced directly by the H atom loss reaction through a barrier at **TS4**, or through pathway **TS2** → $CH_2NCH_3^+$ → **TS5**. By sequential H atom and H_2 molecule elimination reactions, this fragment can produce $HCNCH_2^+$ (m/z = 41) and $HCNC^+$ (m/z = 39) fragments. The fragment with m/z = 40 can not be obtained in this reaction chain due to the high energy of the products. Intermediate $CH_2NCH_3^+$ is also the initial point for the barrierless reaction that gives fragment $CH_2NCH_3^+$ → CH_3^+ (m/z = 15) + CH_2N. The H migration reaction through **TS3** produces intermediate $HCNHCH_3^+$, which is the initial point for three followed reactions producing fragments $HCNH^+$ (m/z = 28) + CH_3, $HCNCH_3^+$ (m/z = 42) + H, and $HCNCH_2^+$ (m/z = 41) + H_2. Low values of vibration frequencies of structure **TS7** provide an unrealistically high value of the rate constant for the channel $HCNHCH_3^+$ → $HCNH^+$ + CH_3 that makes the RRKM calculations incapable to predict branching ratios of these three reactions separately. It was taken into account in Figure 13, where these three channels were joined together. However, the barrier heights of these three reactions let us suppose that $HNCH^+$ preferably is the main dissociation product of the $HCNHCH_3^+$ intermediate. Fragment $HNCH^+$ is relatively stable and needs approximately 170 kcal/mol to be cracked again to produce H^+ (m/z = 1) + HCN and H + HCN^+ (m/z = 27) products with almost equal energies. Based on the experimental observations in Figure 2, although the laser intensity is 1.5×10^{14} W/cm^2, the peak heights of the m/z = 42 and 28 are comparable. Thus, we might conclude that in mass spectra the fragment m/z = 42, whose geometric structure is $CH_2NCH_2^+$, most probably comes from the direct H atom loss reaction $CH_2NHCH_2^+$ → $CH_2NCH_2^+$ + H. The products $HCNCH_2^+$ and $HCNC^+$ are obtained by sequential H and H_2 elimination reactions of $CH_2NCH_2^+$.

TABLE 1: Assignment of the Observed Peaks in the Experimental Mass Spectra Due to Ionization and Dissociation of Pyrrolidine in an Intense Laser Field

m/z	species	origin
71	$C_4H_9N^+$	parent cation
70	$C_4H_8N^+$	H loss from $C_4H_9N^+$ (m/z = 71)
43	$CH_2NHCH_2^+$	primary dissociation of $C_4H_9N^+$ initiated from **i1** or **i4**
42	$CH_2NCH_2^+$	secondary dissociation of $CH_2NHCH_2^+$ (m/z = 43)
	$HCNCH_3^+$	secondary dissociation of $CH_2NHCH_2^+$ (m/z = 43)
41	$HCNCH_2^+$	H loss reaction of $CH_2NCH_2^+$ (m/z = 42)
		Secondary dissociation of $CH_2NHCH_2^+$ (m/z = 43)
39	$HCNC^+$	H_2 loss reaction of $HCNCH_2^+$ (m/z = 41)
28	$HCNH^+$	CH_3 loss reaction of intermediate $HCNHCH_3^+$ (m/z = 43)
27	HCN^+	H loss reaction of $HCNH^+$ (m/z = 28)
15	CH_3^+	CH_2N loss reaction of intermediate $CH_2NCH_3^+$ (m/z = 43)
1	H^+	HCN loss reaction of $HCNH^+$ (m/z = 28)

Table 1 summarizes our assignment of the origin of various peaks observed in the mass spectra. Table 2 gives barrier heights,

TABLE 2: RRKM and VTST Unimolecular Rate Constants (s^{-1}), Reaction Path Degeneracies, and Barrier Heights (kcal/mol) in Dissociation Reactions of Ions $C_4H_9N^+$ and $CH_2NHCH_2^+$ Calculated for Different Values of Internal Energies on the Ground State PES

transition state	reaction	reaction path degeneracy	barriers height, kcal/mol	60 kcal/mol	100 kcal/mol	150 kcal/mol	200 kcal/mol	300 kcal/mol	400 kcal/mol
				$C_4H_9N^+$					
TS1_2, k_{1_2}	**i1 → i2**	4	46.6	9.2×10^4	1.8×10^8	6.8×10^9	4.7×10^{10}	3.7×10^{11}	1.1×10^{12}
TS1_2, k_{2_1}	**i2 → i1**	2	46.6	5.0×10^4	8.3×10^7	3.1×10^9	2.1×10^{10}	1.7×10^{11}	5.0×10^{11}
TS1_3, k_{1_3}	**i1 → i3**	4	42.6	3.2×10^6	2.1×10^9	5.6×10^{10}	3.1×10^{11}	2.0×10^{12}	5.6×10^{12}
TS1_3, k_{3_1}	**i3 → i1**	2	42.6	2.1×10^6	1.0×10^9	2.2×10^{10}	1.1×10^{11}	6.7×10^{11}	1.8×10^{12}
TS1_4, k_{1_4}	**i1 → i4**	2	25.3	1.1×10^{10}	2.2×10^{11}	1.2×10^{12}	3.1×10^{12}	8.8×10^{12}	1.6×10^{13}
TS1_4, k_{4_1}	**i4 → i1**	1	25.3	6.1×10^{10}	1.5×10^{11}	2.4×10^{11}	3.1×10^{11}	4.1×10^{11}	4.8×10^{11}
TS1_7, k_{1_7}	**i1 → P7**	4	28.6	7.4×10^9	3.0×10^{11}	2.5×10^{12}	8.0×10^{12}	2.9×10^{13}	6.0×10^{13}
TS1_9, k_{1_9}	**i1 → P9**	4	59.4		4.0×10^7	1.0×10^{10}	1.6×10^{11}	2.8×10^{12}	1.3×10^{13}
TS2_3, k_{2_3}	**i2 → i3**	2	44.9	3.5×10^5	3.0×10^8	8.0×10^9	4.5×10^{10}	2.8×10^{11}	7.6×10^{11}
TS2_3, k_{3_2}	**i3 → i2**	2	44.9	2.6×10^6	2.9×10^8	8.8×10^9	5.4×10^{10}	3.6×10^{11}	1.1×10^{12}
TS3_7, k_{3_7}	**i3 → P7**	2	39.6		3.0×10^9	5.2×10^{10}	2.5×10^{11}	1.3×10^{12}	3.2×10^{12}
TS4_5, k_{4_5}	**i4 → i5**	4	53.2	6.4×10^4	6.8×10^8	2.1×10^{10}	1.2×10^{11}	6.8×10^{11}	1.7×10^{12}
TS4_5, k_{5_4}	**i5 → i4**	6	53.2	6.2×10^2	2.8×10^7	2.1×10^9	1.8×10^{10}	1.8×10^{11}	6.0×10^{11}
TS4_6, k_{4_6}	**i4 → i6**	1	38.0		1.1×10^{10}	5.8×10^{10}	1.4×10^{11}	3.7×10^{11}	6.1×10^{11}
TS4_6, k_{6_4}	**i6 → i4**	3	38.0		1.5×10^{12}	2.6×10^{12}	3.3×10^{12}	4.5×10^{12}	5.1×10^{12}
TS4_8, k_{4_8}	**i4 → P8**	1	41.9	7.9×10^8	1.1×10^{11}	9.7×10^{11}	2.9×10^{12}	9.3×10^{12}	1.7×10^{13}
TS4_9, k_{4_9}	**i4 → P9**	2	63.4		1.6×10^9	3.4×10^{11}	4.0×10^{12}	5.0×10^{13}	1.6×10^{14}
VTS5_11, k_{5_11}	**i5 → P11**	1	53.2	1.3×10^8	1.4×10^{11}	3.6×10^{12}	2.0×10^{13}	1.2×10^{14}	3.1×10^{14}
VTS6_10, k_{6_10}	**i6 → P10**	1	62.6		2.9×10^9	4.1×10^{11}	2.7×10^{12}	1.5×10^{13}	3.5×10^{13}
				$CH_2NHCH_2^+$					
TS1, k_1	**i43−1 → P43−1**	8	118.7			1.1×10^7	4.9×10^9	5.4×10^{11}	4.3×10^{12}
TS2, k_2	**i43−1 → i43−2**	4	65.2		2.2×10^8	1.6×10^{11}	1.2×10^{12}	8.0×10^{12}	2.1×10^{13}
TS2, k_{-2}	**i43−2 → i43−1**	3	65.2		2.3×10^9	7.5×10^{10}	3.5×10^{11}	1.5×10^{12}	3.0×10^{12}
TS3, k_3	**i43−1 → i43−3**	4	63.9		1.4×10^9	8.4×10^{10}	5.6×10^{11}	3.6×10^{12}	8.6×10^{12}
TS4, k_4	**i43−1 → P43−7**	1	67.2		1.2×10^9	1.5×10^{11}	1.3×10^{12}	1.0×10^{13}	2.8×10^{13}
TS5, k_5	**i43−3 → P43−7**	3	53.6		2.3×10^{11}	3.9×10^{12}	1.2×10^{13}	3.8×10^{13}	6.4×10^{13}
VTS10, k_{10}	**i43−2 → P43−6**	1	102.3			3.9×10^{11}	4.7×10^{12}	1.7×10^{13}	2.7×10^{13}

reaction degeneracies, and rate constants of individual steps of dissociation reactions of $C_4H_9N^+$ and $CH_2NHCH_2^+$.

VI. Conclusions

In this work we studied the ionization and dissociation processes of pyrrolidine by 90 fs intense laser field irradiation at 800 nm for linear and circular polarizations, respectively, in the laser intensity ranging from 2×10^{13} to 4×10^{14} W/cm^2. The g-KFR calculations predict that the dependence of pyrrolidine parent ion yield on laser intensity below the saturation intensity ($\sim 5 \times 10^{13}$ W/cm^2) roughly exhibits a power law of I^5, which is little higher than the experimental observation I^4. It implies that the excited states which are totally neglected in g-KFR theory might take part in the ionization process. Sequentially, we apply the Floquet method to investigate the collective excitation process of neutral pyrrolidine molecule in intense fs LP laser field, and the calculation show that the slopes of 30 excited states can be roughly estimated as 4∼5, showing a reasonable agreement with the experimental observations. Thus aside from the direct ionization (pyrrolidine molecule is ionized from the ground state directly to the continuum state), the excitations of the molecules in the laser field accompanied by further ionization processes are proposed as another main dissociative ionization channel in this case. However, we do not claim it to be a conclusive explanation of ionization processes, and the role of the collective excitation process may be worth further considering by both experimental and theoretical methods.

With regard to dissociation processes, according to the characteristics of the calculated cation absorption spectrum, the weak fragmentation of the pyrrolidine can be interpreted by the absence of the single photon resonance at 800 nm. In addition, some enhancement of fragmentation is observed by the CP laser, especially at high laser intensity. This might be due to the fact that the active energies of the pyrrolidine cation are different for both polarizations. In the present work, we try to interpret this difference from three aspects, such as the Volkov function which describes that the ionized state could behave differently for CP and LP, whether the direction of the laser field is parallel to some induced dipole moment, and the summation of excited states probabilities of pyrrolidine cation is larger in CP laser field. It should also be emphasized that these possibilities are not the definitive conclusions and the mechanism of the fragmentation enhancement by CP laser which need further investigate in detail.

On the other hand, a qualitative understanding of the fs ionization/dissociation mechanisms of pyrrolidine has also been achieved by using the RRKM theory based on the ab initio surfaces. Based on the calculations, the dissociation patterns from the ground state of the molecular cation cannot completely explain the experimental mass spectrum. However, the dissociation via the excited state of the pyrrolidine cation is recognized to be significant to interpret the mass spectra.

To sum up, considering the different characteristics of the mass spectra provided by intense fs laser fields with various conditions (wavelengths, polarizations, pulse durations, intensities and so on), this kind of technique has a great many advantages, and has the potential to develop a new type of mass spectrometry in future.

Acknowledgment. This work was financially supported by the National Science Foundation of China (NSFC) under the Grant 10534010 is acknowledged.

References and Notes

(1) Hankin, S. M.; Villeneuve, D. M.; Corkum, P. B.; Rayner, D. M. *Phys. Rev. Lett.* **2000**, *84*, 5082.

(2) Weber, T.; Giessen, H.; Weckenbrock, M.; Urbasch, G.; Staudte, A.; Spielberger, L.; Jagutzki, O.; Mergel, V.; Vollmer, M.; Dorner, R. *Nature* **2000**, *405*, 658.

(3) Yatsuhashi, T.; Nakashima, N. *J. Phys. Chem. A* **2008**, *112*, 5781.

(4) Palaniyappan, S.; Mitchell, R.; Sauer, R.; Ghebregziabher, I.; White, S. L.; Decamp, M. F.; Walker, B. C. *Phys. Rev. Lett.* **2008**, *100*, 183001.
(5) Zhou, X.; Tong, X. M.; Zhao, Z. X.; Lin, C. D. *Phys. Rev. A* **2005**, *72*, 033412.
(6) Mineo, H.; Nagaya, K.; Hayashi, M.; Lin, S. H. *J. Phys. B: At. Mol. Opt. Phys.* **2007**, *40*, 2435.
(7) Corkum, P. B.; Ellert, C.; Mehendale, M.; Dietrich, P.; Hankin, S.; Aseyev, S.; Villeneuve, D. R. *Faraday Discuss.* **1999**, *113*, 47.
(8) Kaziannis, S.; Kosmidis, C.; Lyras, A. *J. Phys. Chem. A* **2008**, *112*, 4754.
(9) Shimizu, S.; Zhakhovskii, V.; Sato, F.; Okihara, S.; Sakabe, S.; Nishihara, K.; Izawa, Y.; Yatsuhashi, T.; Nakashima, N. *J. Chem. Phys.* **2002**, *117*, 3180.
(10) Shimizu, S.; Zhakhovskii, V.; Murakami, M.; Tanaka, M.; Yatsuhashi, T.; Okihara, S.; Nishihara, K.; Sakabe, S.; Izawa, Y.; Nakashima, N. *Chem. Phys. Lett.* **2005**, *404*, 379.
(11) Barge, V. J.; Hu, Z.; Willig, J.; Gordon, R. J. *Phys. Rev. Lett.* **2006**, *97*, 263001.
(12) Corkum, P. B. *Phys. Rev. Lett.* **1993**, *71*, 1994.
(13) Delone, N. B.; Vladimir, P. K. *Phys. Uspekhi* **1998**, 469.
(14) Guo, C.; Gibson, G. N. *Phys. Rev. A* **2001**, *63*, 040701.
(15) Meyer, M.; Cubaynes, D.; Glijer, D.; Dardis, J.; Hayden, P.; Hough, P.; Richardson, V.; Kennedy, E. T.; Costello, J. T.; Radcliffe, P.; Dusterer, S.; Azima, A.; Li, W. B.; Redlin, H.; Feldhaus, J.; Taieb, R.; Maquet, A.; Grum-Grzhimailo, A. N.; Gryzlova, E. V.; Strakhova, S. I. *Phys. Rev. Lett.* **2008**, *101*, 193002.
(16) Murakami, M.; Tanaka, M.; Yatsuhashi, T.; Nakashima, N. *J. Chem. Phys.* **2007**, *126*, 104304.
(17) Hertel, I. V.; Shchatsinin, I.; Laarmann, T.; Zhavoronkov, N.; Ritze, H. H.; Schulz, C. P. *Phys. Rev. Lett.* **2009**, *102*, 023003.
(18) Wu, D.; Wang, Q. Q.; Cheng, X. H.; Jin, M. X.; Li, X. Y.; Hu, Z.; Ding, D. *J. Phys. Chem. A* **2007**, *111*, 9494.
(19) Wang, Q.; Wu, D.; Jin, M.; Liu, F.; Hu, F.; Cheng, X.; Liu, H.; Hu, Z.; Ding, D.; Mineo, H.; Dyakov, Y. A.; Mebel, A. M.; Chao, S. D.; Lin, S. H. *J. Chem. Phys.* **2008**, *129*, 204302.
(20) Mathur, D.; Hatamoto, T.; Okunishi, M.; Prumper, G.; Lischke, T.; Shimada, K.; Ueda, K. *J. Phys. Chem. A* **2007**, *111*, 9299.
(21) Hankin, S. M.; Villeneuve, D. M.; Corkum, P. B.; Rayner, D. M. *Phys. Rev. A* **2001**, *64*, 013405.
(22) Ammosov, M. V.; Delone, N. B.; Krainov, V. P. *Sov. Phys. JETP* **1986**, *64*, 1191.
(23) Suresh, M.; McKenna, J.; Srigengan, B.; Williams, I. D.; English, E. M. L.; Stebbings, S. L.; Bryan, W. A.; Newell, W. R.; Divall, E. J.; Hooker, C. J.; Langley, A. J. *Nucl. Instrum. Methods in Phys. Res. B* **2005**, *235*, 216.
(24) Talebpour, A.; Bandrauk, A. D.; Vijayalakshmi, K.; Chin, S. L. *J. Phys. B: At. Mol. Opt. Phys.* **2000**, *33*, 4615.
(25) Mass Spectra. *NIST Chemistry WebBook* Linstrom, P. J.; Mallard, W. G., Eds.; NIST Standard Reference Database; National Institute of Standards and Technology: Gaithersburg, MD, 2005; Vol. 69, p 20899.
(26) Brabec, T.; Cote, M.; Boulanger, P.; Ramunno, L. *Phys. Rev. Lett.* **2005**, *95*, 073001.
(27) Tong, X. M.; Lin, C. D. *J. Phys. B: At. Mol. Opt. Phys.* **2005**, *38*, 2593.
(28) Keldysh, L. V. *Sov. Phys. JETP* **1965**, *20*, 1307.
(29) Mishima, K.; Nagaya, K.; Hayashi, M.; Lin, S. H. *Phys. Rev. A* **2004**, *70*, 063414.
(30) Nagaya, K.; Mineo, H.; Mishima, K.; Villaeys, A. A.; Hayashi, M.; Lin, S. H. *Phys. Rev. A* **2007**, *75*, 013402.
(31) Kjeldsen, T. K.; Bisgaard, C. Z.; Madsen, L. B.; Stapelfeldt, H. *Phys. Rev. A* **2003**, *68*, 063407.
(32) Usachenko, V. I.; Chu, S.-I. *Phys. Rev. A* **2005**, *71*, 063410.
(33) Gibson, G. N.; Fang, L.; Moser, B. *Phys. Rev. A* **2006**, *74*, 041401.
(34) Teranishi, Y.; Hayashi, M.; Kong, F.; Chin, S. L.; Chao, S. D.; Mineo, H.; Lin, S. H. *Mol. Phys.* **2008**, *106*, 333.
(35) Faisal, F. H. M. *J. Phys. B: At. Mol. Opt. Phys.* **1973**, *6*, L89.
(36) Reiss, H. R. *Phys. Rev. A* **1980**, *22*, 1786.
(37) Mineo, H.; Chao, S. D.; Nagaya, K.; Mishima, K.; Hayashi, M.; Lin, S. H. *Chem. Phys. Lett.* **2007**, *439*, 224.
(38) Chu, S.-I.; Telnov, D. A. *Phys. Rep.* **2004**, *390*, 1.
(39) DeWitt, M. J.; Levis, R. J. *J. Chem. Phys.* **1999**, *110*, 11368.
(40) Frisch, M. J.; Schlegel, G. W. T. H. B.; Scuseria, G. E.; Robb, M. A.; Cheeseman, J. R.; Montgomery Jr., J. A.; Vreven T.; Kudin, K. N.; Burant, J. C.; Millam, J. M.; Iyengar, S. S.; Tomasi, J.; Barone, V.; Mennucci, B.; Cossi, M.; Scalmani, G.; Rega, N.; Petersson, G. A.; Nakatsuji, H.; Hada, M.; Ehara, M.; Toyota, K.; Fukuda, R.; Hasegawa, J.; Ishida, M.; Nakajima, T.; Honda, Y.; Kitao, O.; Nakai, H.; Klene, M.; Li, X.; Knox, J. E.; Hratchian, H. P.; Cross, J. B.; Adamo, C.; Jaramillo, J.; Gomperts, R.; Stratmann, R. E.; Yazyev, O.; Austin, A. J.; Cammi, R.; Pomelli, C.; Ochterski, J. W.; Ayala, P. Y.; Morokuma, K.; Voth, G. A.; Salvador, P.; Dannenberg, J. J.; Zakrzewski, V. G.; Dapprich, S.; Daniels, A. D.; Strain, M. C.; Farkas, O.; Malick, D. K.; Rabuck, A. D.; Raghavachari, K.; Foresman, J. B.; Ortiz, J. V.; Cui, Q.; Baboul, A. G.; Clifford, S.; Cioslowski, J.; Stefanov, B. B.; Liu, G.; Liashenko, A.; Piskorz, P.; Komaromi, I.; Martin, R. L.; Fox, D. J.; Keith, T.; Al-Laham, M. A.; Peng, C. Y.; Nanayakkara, A.; Challacombe, M.; Gill, P. M. W.; Johnson, B.; Chen, W.; Wong, M. W.; Gonzalez, C. and Pople, J. A. , Gaussian, Inc., Pittsburgh, 2003.
(41) Gorelsky, S. p. S. I. , revision 4.0, http://www.sg-chen.net An absorption profile is calculated as a sum of Gaussian bands, data points are created every 100 cm-1, width at half-height = 3000 cm-1. Individual contributions are printed only if they exceed the 1/10 000th of the maximum molar absorptivity in the selected frequency range.
(42) Pickett, L. W.; Corning, M. E.; Wieder, G. M.; Semenow, D. A.; Buckley, J. M. *J. Am. Chem. Soc.* **1953**, *75*, 1618.
(43) Rajgara, F. A.; Krishnamurthy, M.; Mathur, D. *J. Chem. Phys.* **2003**, *119*, 12224.
(44) Rajgara, F. A.; Krishnamurthy, M.; Mathur, D. *Phys. Rev. A* **2003**, *68*, 023407.
(45) Dyakov, Y. A.; Mebel, A. M.; Lin, S. H.; Lee, Y. T.; Ni, C.-K. *J. Phys. Chem. A* **2007**, *111*, 9591.
(46) Becke, A. D. *J. Chem. Phys.* **1993**, *98*, 5648.
(47) Lee, C.; Yang, W.; Parr, R. G. *Phys. Rev. B* **1988**, *37*, 785.
(48) Baboul, A. G.; Curtiss, L. A.; Redfern, P. C.; Raghavachari, K. *J. Chem. Phys.* **1999**, *110*, 7650.
(49) Curtiss, L. A.; Raghavachari, K.; Redfern, P. C.; Baboul, A. G.; Pople, J. A. *Chem. Phys. Lett.* **1999**, *314*, 101.
(50) MOLPRO is a package of ab initio programs written by Werner H.-J. and Knowles P. J. with contributions from. : Almlöf, J. A., R. D.; Deegan, M. J. O.; Elbert, S. T.; Hampel, C.; Meyer, W.; Peterson, K.; Pitzer, R.; Stone, A. J.; Taylor, P. R. and Lindh, R.
(51) Sharifi, M.; Kong, F.; Chin, S. L.; Mineo, H.; Dyakov, Y.; Mebel, A. M.; Chao, S. D.; Hayashi, M.; Lin, S. H. *J. Phys. Chem. A* **2007**, *111*, 9405.

JP901857K